Global view of the nighttime low-latitude ionosphere by the IMAGE/FUV 135.6 nm observations

Eiichi Sagawa and Takashi Maruyama

Communications Research Laboratory, Tokyo, Japan

Thomas J. Immel, Harald U. Frey, and Stephen B. Mende

Space Sciences Laboratory, University of California, Berkeley, USA

[1]   The FUV Spectrographic Imager (FUV/SI) onboard the IMAGE satellite takes images at two wavelengths (121.8 nm: SI-12 and 135.6 nm: SI-13). The SI-13 images of the low latitude region at night clearly show the intertropical FUV arcs corresponding to the equatorial anomaly (EA) in the ionosphere. The two-minute cadence of the instrument provides a unique data set of the nighttime low-latitude ionosphere. We compare the IMAGE observations of the OI 135.6 nm nightglow with the model emission intensities calculated by using the SAMI2 ionosphere model. The comparison shows that although both the FUV observation and the model give comparable emission intensities near the EA peak, the two differ in terms of their latitudinal and local time dependences. Large-scale ($\sim$1000 km) longitudinal wavy structures are often seen in OI 135.6 nm images. These structures drift eastward with a phase velocity of $\sim$100 m/s. The structure may be due to the plasma density perturbations generated by acoustic gravity waves through amplification by the spatial resonance and the Rayleigh-Taylor (R-T) instability. This is a common structure seen in the pre-midnight sector of FUV/SI images regardless of longitude.   *INDEX TERMS:* 0310 Atmospheric Composition and Structure: Airglow and aurora; 2415 Ionosphere: Equatorial ionosphere; 2423 Ionosphere: Ionization mechanisms; 2427 Ionosphere: Ionosphere/atmosphere interactions (0335); 2494 Ionosphere: Instruments and techniques. **Citation:** Sagawa, E., T. Maruyama, T. J. Immel, H. U. Frey, and S. B. Mende, Global view of the nighttime low-latitude ionosphere by the IMAGE/ FUV 135.6 nm observations, *Geophys. Res. Lett.*, *30*(10), 1534, doi:10.1029/2003GL017140, 2003.

1.   Introduction

[2]   Satellite imaging of OI 135.6 nm FUV light is a powerful tool for investigating global characteristics of the earth's upper atmosphere. *Huffman* [1992] pointed out that UV imaging methods will be a valuable element in the future global space weather system in which ionospheric and atmospheric conditions are continuously monitored. Auroras have been investigated through this technique, partly because of their strong emission at 135.6 nm. On the other hand, even though the mid- and low-latitude ionosphere can also be a good target, the low intensity of OI 135.6 nm emission has discouraged detailed study. The

OI 135.6 nm emission in the nighttime ionosphere comes mostly from recombination of the atomic oxygen ion. Although there exists another reaction of minor importance (ion-ion neutralization [*Hanson*, 1970]), the 135.6 nm emission is mostly determined by the square of the electron density because the oxygen ion is a major ion species near the *F*-layer peak. The OGO-4 satellite first observed the OI 135.6 nm emission, which showed that the low-latitude ionosphere is characterized by two emission peaks located $10°-20°$ from the geomagnetic equator. This corresponds to peaks of the plasma density of the equatorial anomaly (EA) [*Hicks and Chubb*, 1970; *Barth and Schaffner*, 1970]. Since those early measurements, several OI 135.6 nm measurements have been reported. Recently, *Huba et al.* [2002] reported that the O^+ density deduced from the OI 135.6 nm limb scan data agrees well with the SAMI2 ionosphere model. These prove that the remote sensing of the OI 135.6 nm emission is a powerful tool for probing the nighttime ionosphere from space. Now the IMAGE satellite launched in 2000 [*Burch*, 2000] brings the global imaging of the ionosphere by the OI 135.6 nm emission.

[3]   The FUV onboard IMAGE has three cameras for imaging the upper atmosphere at three wavelengths. One of these (SI-13) has the pass band centered at 135.6 nm with an 8-nm bandwidth [*Mende et al.*, 2000]. Although the primary objective of the instrument is to capture auroral images, the instrument is sensitive enough to image the low-latitude ionosphere at night. In this paper, we examine the characteristics of 135.6 nm images of the low-latitude ionosphere taken by the FUV/SI-13 instrument by making a comparison with the model emission calculated by using the SAMI2 ionosphere model, and also describe a large-scale structure commonly seen in the pre-midnight sector of FUV/SI images regardless of longitude.

2.   Comparison With the SAMI2 Model

[4]   Figure 1 shows an example of a FUV/SI-13 image of the low-latitude ionosphere taken on April 24, 2002 at 18:42 UT. Geomagnetic activity was quiet at the time of the observation, as can be confirmed from the fact that no clear aurora oval is seen in the figure. The North Pole is located at the middle near the left edge, the equator runs almost vertically at the right, and the dusk is toward the bottom in the image. Two longitudinally extended bright bands of the OI 135.6 nm emission can be clearly seen. The bands correspond to the plasma density enhancement of EA at both sides of the equator. The two-band structure com-
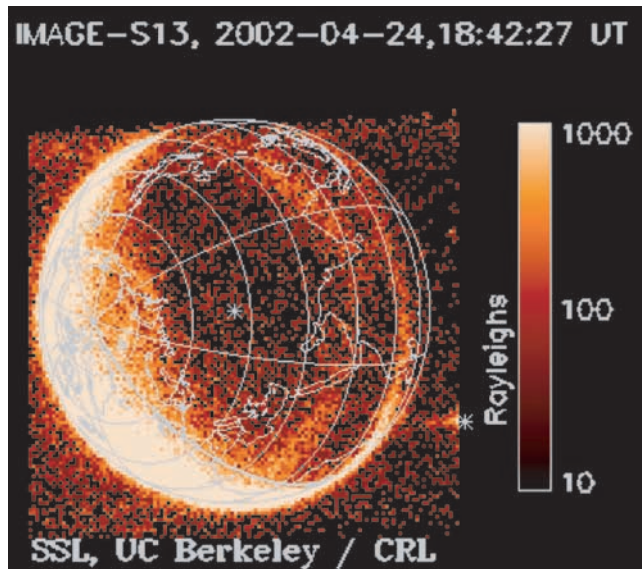
Figure 1. A 135.6 nm image observed by IMAGE FUV/SI on April 24, 2002 at 18:42 UT. The bright region is the sunlit hemisphere of the earth. The bright band at the top is an artifact caused by the process to convert the raw image into a calibrated image. The two almost vertical bands in the right part of the image correspond to plasma density enhancements of EA.

monly appeared in the FUV images taken from March to June 2002 when the satellite was located in the night side.

[5] We compare the SI-13 observation with the column emission calculated by using the SAMI2 ionosphere model. The SAMI2 model calculates the ionospheric plasma along the earth's dipole magnetic field line from hemisphere to hemisphere, and includes ion inertia in the ion momentum equation. An empirical electric field model [*Scherliess and Fejer*, 1999] can be used to calculate the ExB drift of a flux tube. Empirical models provide neutral densities and the wind field. Note that by adopting the offset dipole magnetic field model, the SAMI2 includes effects of varying declination angle longitudinally. The model calculation is carried out for field lines located from $-40°$ to $40°$ in latitude, and from $0°$ to $360°$ in longitude under conditions as of April 24, 2002 at 17:00 UT. Input parameters to SAMI2 are: $F_{10.7}$

$= 177$, $F_{10.7A}$ (3 month average) $= 198$, and $A_p = 7$. From the model ionosphere, we calculate the 135.6 nm column emission by integrating the volume emission rates vertically by using the following fomula [*Dymond et al.*, 1997]:

$$I = \int \alpha_{1356} n(O^+) n(e) dz + \int \frac{\beta_{1356} K_1 K_2 n(O) n(O^+) n(e)}{K_2 n(O^+) + K_3 n(O)} dz \quad (1)$$

where α_{1356} is the radiative reaction rate 6.5×10^{-13} cm^{-3}s^{-1}; β_{1356} is the fraction of neutralization 0.54; and the coefficients $k1$, $k2$, $k3$ of neutralization reactions are 1.3×10^{-15}, 1.5×10^{-7}, and 1.4×10^{-10} cm^{-3}s^{-1}, respectively [*Tinsley and Bittencourt*, 1975]. Densities of electron, O$^+$, and O ($n(e)$, $n(O^+)$, and $n(O)$ respectively) are obtained from the model. No provision for multiple scattering is taken into account, because the effect of multiple scattering is less than 20% for the 135.6 nm emission [*Meier*, 1991]. The contribution of the ion-ion neutralization is estimated by using the model ionosphere to be up to 10% of the column emission.

[6] To deduce the experimental column emission, we multiply the observed emission intensity by the cosine of the viewing angle measured from the nadir to the observation points. This approximation is justified as follows. The 135.6 nm volume emission rate is, as a first approximation, proportional to the square of the plasma density. Therefore, the majority of the column emission originates from ~100 km altitude range containing the F-layer peak. This, in turn, justifies the use of a simple geometrical correction, which assumes a horizontally uniform emission layer whose thickness is similar in scale to the ionosphere thickness. Note that this assumption becomes invalid near the edge of the FUV/SI field of view where the view angle becomes too large.

[7] Figure 2 compares the FUV observation with the model emission at the four local times plotted on the geographic latitude axis. The observation used in the comparison was carried out from 12:00 to 12:20 UT on April 24, 2002. Ten images are averaged to improve the signal-to-noise ratio. Image pixels are projected onto the geographic coordinates so that we could deduce the latitudinal profiles of the 135.6 nm column emission. For each local time, the corresponding longitude data are averaged over 10° in longitude; e.g., for 20 LT, from 40° to 50°E. The figure indicates that the absolute intensity is comparable (~100 R)
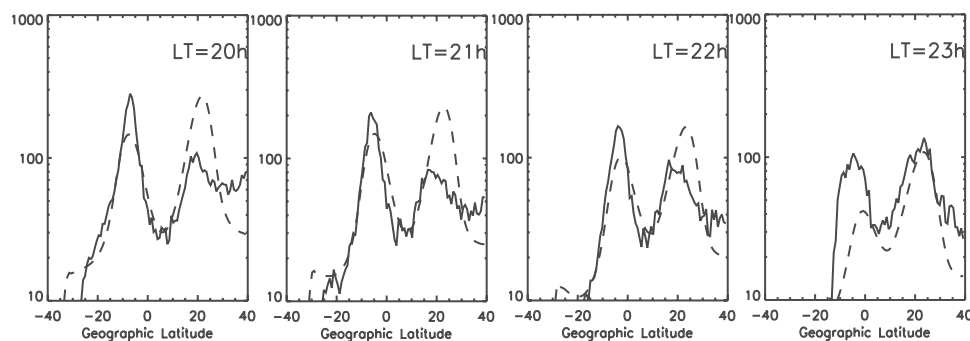

Figure 2. Comparison of the FUV/SI 135.6 nm emission (solid lines) with the model emission (dashed lines) calculated by using the SAMI2 ionosphere model. Ten FUV/SI measurements done from 12:00 to 12:20 UT on April 24, 2002 were averaged. The four plots compare the latitudinal distribution of the 135.6 nm column emission at four local times from 20 to 23 LT. The vertical axis is the emission intensity in Rayleighs, and the horizontal axis is the geographic latitude. Each FUV/SI data was integrated longitudinally for 10°.
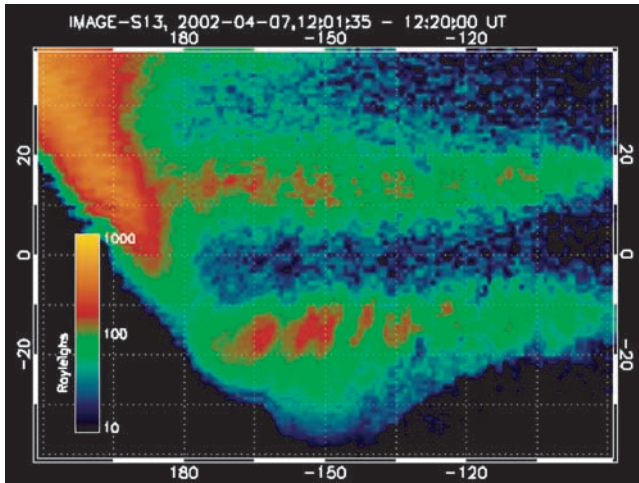
Figure 3. Expanded view of the FUV/SI image in the geomagnetic coordinates. The vertical axis is the magnetic latitude ($-40°-40°$) and the horizontal axis is the magnetic longitude ($150°E-90°W$). The FUV images are integrated for ten measurements (~20 minutes). The bright area in the upper left corner is the sunlit region, and the dark area near the bottom left corner is the region outside of the FUV's field of view.

near the EA peak, and that, in general terms, the experiment and the model give similar latitudinal profiles. However, there exist some differences in the latitude and local time dependences. While the model predicts an almost symmetric latitude profile for 20, 21, and 22 LT, the FUV/SI observation shows an asymmetric distribution where the southern (winter) EA peak is more intense than the northern (summer) peak. The last panel (23LT) of Figure 2 shows a large difference between the observed and model emission profiles. This shows that while the model predicts a rapid decline of the EA after 22 LT, the EA does not decline to the extent the model predicts, and even increases with local time in the northern hemisphere. This local time dependence can be seen in Figure 1 in which the bright emission bands continued beyond midnight, in particular the northern band intensified after gradual dimming at dusk.

3. Large-Scale Longitudinal Wave Structure

[8]   Figure 3 shows an expanded view of the 135.6 nm image averaged from 12:00 to 12:20 UT on April 7, 2002. The image is projected onto the geomagnetic coordinate. The dark part near the left bottom corner corresponds to the region outside of the instrument's field of view. Two bands of the 135.6 nm emission clearly show longitudinal modulation with the scale of ~10°. It can also be seen that the structure is roughly in phase at both hemispheres. This suggests that the structure is basically field-aligned.

[9]   The IMAGE satellite near its apogee can observe the earth for several hours continuously. In the top panel of Figure 4, we have plotted eight longitudinal profiles of the emission intensity averaged from $10°$ to $20°$ geomagnetic latitudes. These were observed from 12:00 to 15:00 UT on April 7, 2002, and plotted every 20 minutes. The solid line labeled as '12:09 UT' plots a profile obtained first with the scale indicated by the vertical axis. Profiles observed

successively are divided by 2^{n-1} for the nth observation. A large-scale perturbation of the emission intensity is clearly seen in addition to a gradual decrease due to the local time change. The amplitude of the intensity modulation shown in the figure is less than about 50%, which corresponds to the plasma density modulation of about 25%. The figure also shows an apparent eastward drift of the pattern. In the bottom panel, we plotted the longitudes of the density depression seen in the top panel versus time after 12:00 UT. The same symbols are used to indicate the location of corresponding dips in the intensity modulation. Also plotted in the panel are least-squares fitted straight lines. The estimated eastward drift velocities ranged from 113 to 158 m/s at the equator.

[10]   It is possible that the depression of the plasma density shown in Figure 3 may include plasma bubbles. However,
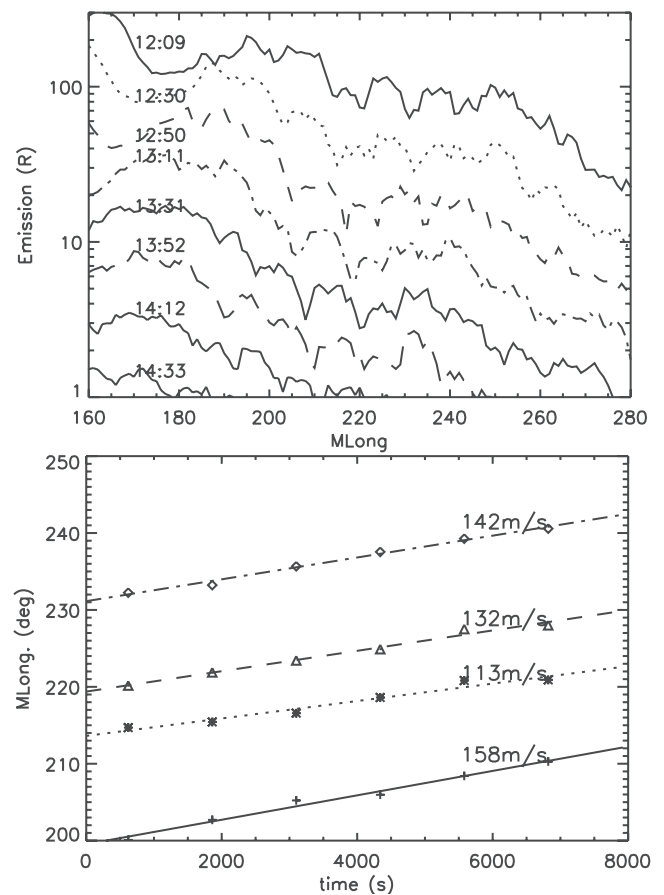

Figure 4. Top panel: Longitudinal slice of the 135.6 nm column emission from 12:00 to 15:00 UT on April 7, 2002. The eight lines plot the emission intensity longitudinally. Ten images were averaged for each profile and sampled with approximately 20-minute intervals. The solid line plots data from 12:09 UT with the scale shown in the vertical axis, and successive data are plotted by dividing by 2^{n-1} for the nth data. Bottom panel: Plots of points corresponding to the first six measurements shown in the top panel. The vertical axis is the magnetic longitude, and the horizontal axis is the time elapsed since 12:00 UT on April 24, 2002. Symbols show data points and the lines are the least squares fit to the data. The number attached to each line is the estimate eastward drift velocity at the equator.

the spatial resolution of the instrument is not good enough to resolve a single plasma bubble, which can sometimes have a spatial size much smaller than 100 km. At this period the FUV images were taken over the South East Asia. Scintillation measurements at Bangkok (13.7°N) in Thailand detected weak scintillation (S4 ≈ 0.3) at 1.7 GHz from 10:40 to 15:20 UT (*M. Nakamura*, Communications Research Laboratory, personal communication, 2003). This fact suggests the plasma irregularities certainly coexisted with the structure imaged by FUV. The observed structure has the scale length of ∼1000 km. It is well established that the plasma bubbles and plasma irregularities occur in quasi periodic batches in the equatorial ionosphere, of which the scale length is similar to what we observed [*Rotteger*, 1973].

4. Discussion and Summary

[11] Global images of the 135.6 nm emission from the nighttime low-latitude ionosphere were observed by the IMAGE satellite. Observations continuing for several hours with high cadence (2 minutes) make the FUV data quite unique. The comparison with the model emission calculated by using the SAMI2 ionosphere model yielded comparable intensities, although the latitude and local time dependences differed. From the 630-nm emission observed by the WINDII instrument on board UARS, *Thuillier et al.* [2002] confirmed earlier results that the emission intensity at the EA peak is stronger in the winter hemisphere, and that this is consistent with the simultaneous neutral wind measurements. They concluded that the interhemispheric plasma flow driven by the neutral wind field causes the asymmetric distribution of the plasma density. Our result is qualitatively consistent with the WINDII result. This suggests that the neutral wind field used in the model calculation is not adequate. In the comparison of O^+ density from ARGOS LORASS data analysis and SIMA2 model results, *Huba et al.* [2002] pointed out that the model results are sensitive to the electric field and neutral wind field models, particularly near the geomagnetic equator. In the model run, we used HWM93 wind model. Because the model could use the different neutral wind model, further comparison of the FUV/SI data and the SMAI2 model will provide an important contribution in understanding the behavior of the low-latitude ionosphere which is strongly affected by the neutral atmosphere.

[12] The FUV/SI observations show that there exists wavy plasma density perturbations with a ∼1000 km scale and it drifts eastward with a velocity of ∼100 m/s. This is a very common feature seen in the FUV/SI images. The longitude structure in the low latitude ionosphere has been discussed extensively, in particular, with the relationship to plasma bubbles and the spread-*F*. AE-E observation of a large-scale density perturbation was reported by *Singh et al.* [1997] who observed plasma density modulation on a ∼1000-km scale and found plasma bubbles at the bottom of these density perturbations. Similar spatial scale size was also observed in the ionospheric irregularities by ground-based observations of the transequatorial HF propagation [*Rotteger*, 1973]. Plasma bubbles are known to develop through R-T instability at the bottom of the *F*-layer. For this instability to grow, density modulation must occur at the bottom of the *F*-layer as a seeding mechanism. A possible candidate for this is the density perturbation caused by acoustic gravity waves. *Whitehead* [1971] pointed out that if the drift velocity of the plasma coincides with the phase velocity of gravity waves, a well-developed density modulation would result in (spatial resonance). *Huang and Kelley* [1996] have shown through simulation that gravity waves produce a large density modulation at the bottom of the *F*-layer, even without the spatial resonance, because of the R-T instability triggered by the small density perturbation. Because the plasma drift velocity and the neutral wind speed do not necessarily match each other, the spatial resonance condition could not always be met. Collaboration of the global imaging of the low latitude ionosphere by FUV and ground based observations with high spatial resolution will provide a clue to the seeding mechanism of the plasma bubbles and the spread-*F*.

References

Barth, C. A., and S. Schaffner, Ogo4 spectrometer measurements of the tropical ultraviolet airglow, *J. Geophys. Res.*, 75, 4299–4306, 1970.

Burch, J., Image mission overview, *Space Sci. Rev.*, 91, 1–14, 2000.

Dymond, K. F., S. E. Thonnard, R. P. McCoy, and R. J. Thomas, An optical remote sensing technique for detecting nighttime *F* region electron density, *Radio Sci.*, 32, 1985–1996, 1997.

Hanson, W. B., A comparison of the oxygen ion-ion neutralization and radiative recombination mechanism for producing the ultraviolet nightglow, *J. Geophys. Res.*, 75, 4343–4346, 1970.

Hicks, G. T., and T. A. Chubb, Equatorial aurora/airglow in the far ultraviolet, *J. Geophys. Res.*, 75, 6233–6248, 1970.

Huang, C.-S., and M. C. Kelley, Nonlinear evolution of equatorial spread *F*, 1. On the role of plasma instabilities and spatial resonance associated with gravity wave seeding, *J. Geophys. Res.*, 101, 283–292, 1996.

Huba, J. D., G. Joyce, and J. A. Fedder, Sami2 is another model of the ionosphere (SAMI2): A new log-latitude ionosphere model, *J. Geophys. Res.*, 105, 23,035–23,053, 2000.

Huba, J. D., K. F. Dymond, G. Joyce, A. A. Budzien, S. E. Thonnard, J. A. Fedder, and R. P. McCoy, Comparison of O^+ demsity from ARGOS LORAAS data analysis and SAMI2 model results, *Geophys. Res. Lett.*, 29, 10.1029/2001GL013089, 2002.

Huffman, R. R., *Atmospheric ultraviolet remote sensing*, Academic Press Inc., San Diego, 1992.

Meier, R. R., Ultraviolet spectroscopy and remote sensing of the upper atmosphere, *Space Sci. Rev.*, 58, 1–186, 1991.

Mende, S. B., et al., Far ultraviolet imaging from the IMAGE spacecraft. 3. Spectral imaging of Lyman-α and OI 135.6 nm, *Space Sci. Rev.*, 91, 287–318, 2000.

Rotteger, J., Wavelike structure of large scale equatorial spread *F* irregularities, *J. Atmos. Terr. Phys.*, 35, 1195–1206, 1973.

Scherliess, L., and B. G. Fejer, Radar and satellite global equatorial *F* region vertical drift model, *J. Geophys. Res.*, 104, 6829–6842, 1999.

Singh, S., F. S. Johnson, and R. A. Power, Gravity wave seeding of equatorial plasma bubbles, *J. Geophys. Res.*, 102, 7399–7410, 1997.

Thuillier, G., R. H. Wiens, G. G. Sphered, and R. G. Roble, Photochemistry and dynamics in thermospheric intertropical arcs measured by the WIND imaging interferometer on board UARS: A comparison with TIE-GCM simulations, *J. Atoms. Solar-Terr. Phys.*, 64, 405–415, 2002.

Tinsley, B. A., and J. A. Bittencourt, Determination of F region height and peak electron density at night using airglow emissions from atomic oxygen, *J. Geophys. Res.*, 80, 2333–2337, 1975.

Whitehead, J. D., Ionization disturbances caused by gravity waves in the presence of an electrostatic field and background wind, *J. Geophys. Res.*, 76, 238–241, 1971.

———————
E. Sagawa and T. Maruyama, Communications Research Laboratory, 4-2-1 Koganeishi, Nukuikitamachi, Tokyo 184-8795, Japan. (esagawa@crl.go.jp)

T. J. Immel, H. U. Frey, and S. B. Mende, Space Science Laboratory, University of California, Berkeley, CA 94720, USA. (immel@ssl.berkeley.edu)